COMPDYN 2015
5th ECCOMAS Thematic Conference on
Computational Methods in Structural Dynamics and Earthquake Engineering
M. Papadrakakis, V. Papadopoulos, V. Plevris (eds.)
Crete Island, Greece, 25–27 May 2015

EXPERIMENTAL AND ANALYTICAL INVESTIGATION OF AN UNCONVENTIONAL, ROCKING TYPE RESPONSE MECHANISM FOR EARTHQUAKE-RESISTANT BRIDGES

Vasileios G. Pilitsis, Ioannis A. Tegos, Vassilis K. Papanikolaou and Kosmas-Athanasios Stylianidis

Aristotle University of Thessaloniki
Faculty of Engineering
School of Civil Engineering
Laboratory of Reinforced Concrete and Masonry
vpilitsi@civil.auth.gr
itegos@civil.auth.gr
billy@civil.auth.gr
kcstyl@civil.auth.gr

Keywords: Integral bridges, reinforcement bond, rocking, experimental, seismic.

Abstract. *In the present study a new technique is investigated, which takes advantage of the rocking principle for the treatment of the two ambivalent demands in bridge designing, i.e. due to seismic and serviceability actions. The idea is based on the formation of cracks only in two positions on each bridge pier, which are the pier cross-sections in contact with the deck and the pile cap respectively, excluding the possibility of cracking in the mid-length of the piers. The possibility of flexural crack formation in one of these cross-sections was examined experimentally in order to reach the above objective. This was achieved through partial suppression of the longitudinal reinforcement bond with the surrounding concrete. In order to confirm the feasibility of the above objective and to verify the influence of the bond suppression on all three response indexes, namely strength, stiffness and ductility, eight experimental specimens in the form of cantilevers, representing ductile bridge piers, were prepared. The varying parameter was the shear span ratio. Useful results were observed regarding the three response indexes and interesting conclusions were obtained.*

1 INTRODUCTION

The basic objective of a seismic isolation system is to increase the fundamental period of the structure and reduce the design seismic acceleration. This phenomenon is known in the literature as "period shift effect" [1]. Increasing the fundamental period may be achieved by using seismic isolation devices, such as elastomeric bearings. A new technique for precast concrete bridges is the use of rocking as seismic isolation. Pure precast elements are connected though unbonded post-tensioning techniques; the inelastic demand is accommodated within the connection where a "controlled rocking" motion occurs with opening and closing of existing gap [2], [3], [4].

An alternative to the rocking technique method is the canceling of total bond (i.e. adhesive, friction and mechanical interlock) between steel rebar and the surrounding concrete in the connection joint of the deck-pier and its pier-pile cap. This adjustment aims at the improvement of the response, compared to with the corresponding monolithic connection, regarding the serviceability and seismic requirements, while reducing cost. The innovation consists in the way of anchoring the longitudinal reinforcement underlying pile-cap and the overlying deck of the bridge (Fig. 1). According to Fig. 1, longitudinal reinforcement is overlapped with awaiting rebars which are anchored to the pile cap in a way where a part of reinforcement length, nearest to the web of the pier, is not integrated into the surrounding concrete. Similarly, the outbound awaiting rebars on the head of the pier are not anchored in their full length to the deck, but only in their upper part. The construction joint in the footing of the pier is inserted in the pile cap for 15 cm, while the joint at the heading of the pier is inserted for 15 cm in the deck. These measures aim to prevent drifts at the interface of construction joints. The measures taken in order to prevent full fixity of the longitudinal reinforcement in the areas of anchorages, lead to the partial release regarding the rotations of the end-part sections of the piers. Via these rotations, the stiffness of the piers can be dramatically reduced for the benefit of serviceability requirements which are associated with alleviating stresses arising from the constraints caused by the expansion/contraction of the deck. By this generated high degree of flexibility, a satisfactory degree of seismic isolation is also achieved, since it leads to the significant increase of the fundamental period [5].

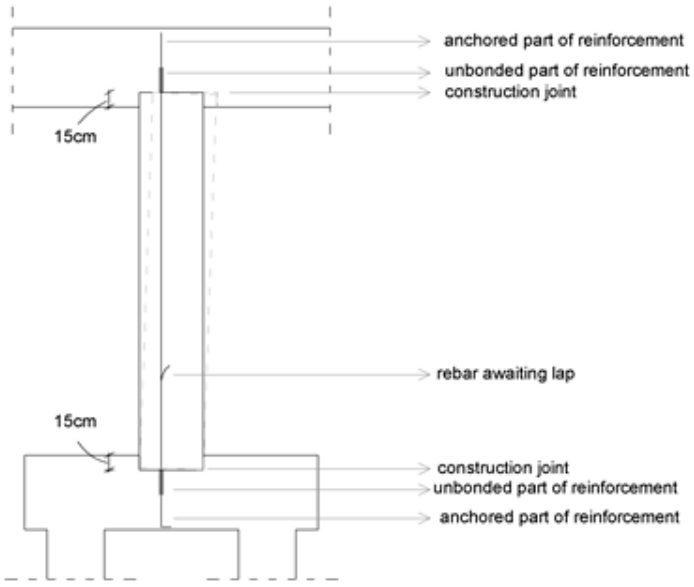

Figure 1: Anchorage conditions of typical reinforcement.

An experimental evaluation of the mechanical behavior of this novel type of joint connection is attempted in this study. In particular, three response indexes are examined namely strength, stiffness and ductility. Furthermore, the influence of reinforcement to concrete bond suppression is examined on energy dissipation capacity and constant performance of the piers during cyclic loading.

2 SPECIMEN GEOMETRY

Eight cantilever specimens were prepared in 1:3 scale corresponding to the dimensions of two typical cases of a wall-web of an abutment with pinned base: (a) a flexible wall-web with height of 4.50 m and thickness of 50 cm and (b) a stiffer wall-web with height of 1.50 m and thickness of 50 cm. Since it is difficult to achieve full fixity conditions in laboratory, the eight cantilever specimens were formed as four beams simply supported in both ends. Two of the beams had length of 3.20 m and while the other two had length of 1.20 m respectively to the represented cases. Each beam consists of two cantilevers of net length of 0.375 m for case (a) and 1.375 m for the case (b) (Fig. 2, Fig. 3). The width of the beams was chosen 36 cm for proper mounting of the loading device (actuator) to the beams. In the midspan of each beam, a stiff zone is formed with thickness of 35 cm and length of 25 cm, in which the external load is imposed and by which the full fixity of each cantilever is achieved. The diagrams of internal forces and the elastic line of a simply supported beam with a concentrated load in the midspan is equivalent to the composition of two cantilevers diametrically opposed with concentrated load at one end-part and equal to the half of the simply supported beam's load. The hinge supports were implemented at 10 cm from the edges of each beam.

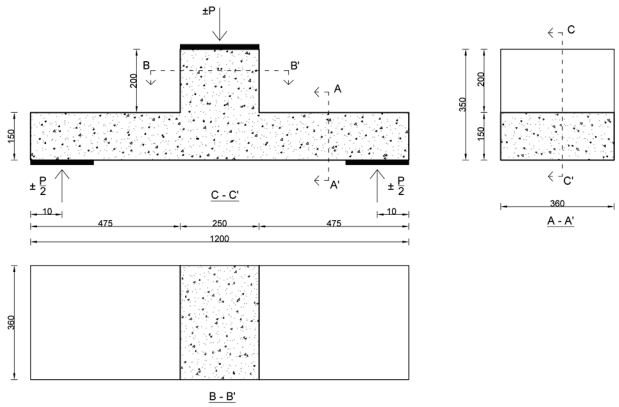

Figure 2: Geometry of the short span specimens.

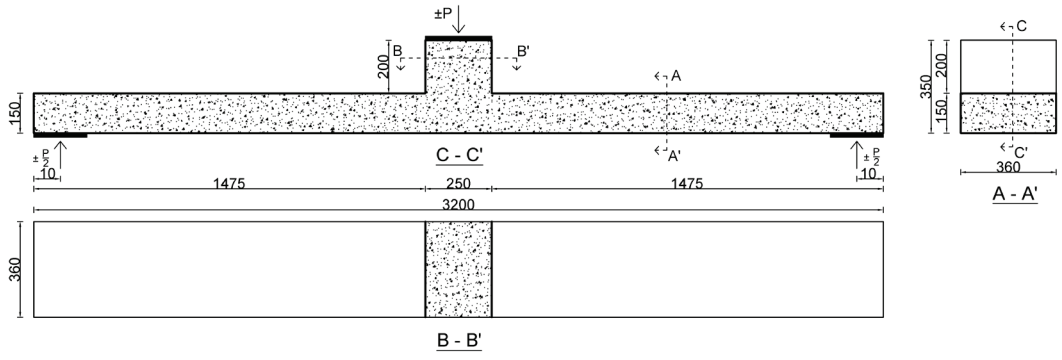

Figure 3: Geometry of the long span specimens.

3 REINFORCEMENT DETAILING AND MATERIAL PROPERTIES

Longitudinal reinforcement of each specimen consists of ten Ø10. That corresponds to a longitudinal reinforcement ratio of ρ_l=1.45 %. The transverse reinforcement used in both types of specimens accrued so that to ensure that the specimens will experience flexural failure. The concrete cover was equal to 1.0 cm in both cases.

Two of the specimens, namely one short specimen (low shear span ratio) and one long specimen (high shear span ratio), were reinforced without suppressing bond between concrete and reinforcement. In the other two specimens, the total bond of longitudinal reinforcement with the surrounding concrete was suppressed in specific regions. In the short specimen the suppression took place in length of 65mm symmetrically extended to the mid-length of the beam (Fig. 4). In the long specimen the suppression took place in length of 205 cm also symmetrically extended to the mid-length of the beam (Fig. 5). The reinforcement to concrete bond suppression was achieved by meticulous wrapping of the reinforcement rebar with polyethylene sheets (Fig. 6).

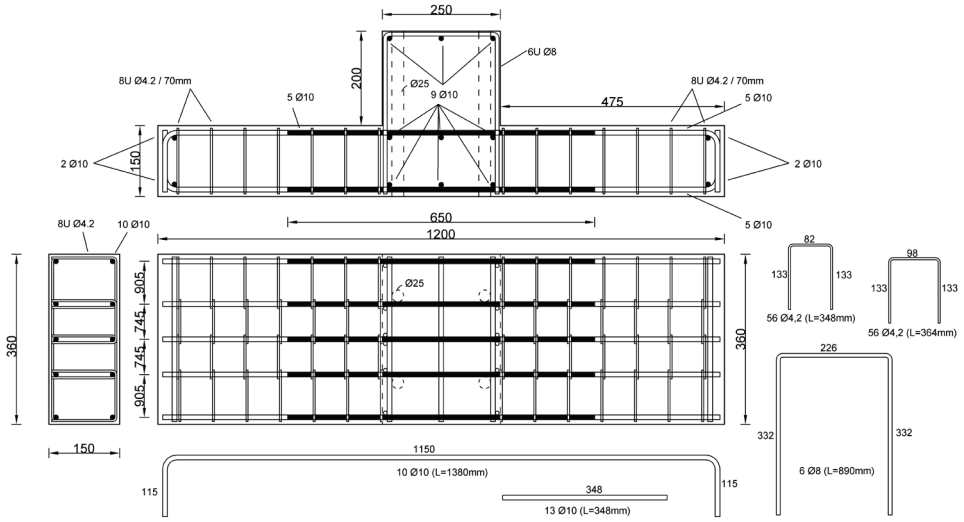

Figure 4: Unbonded reinforcement of the short span specimen.

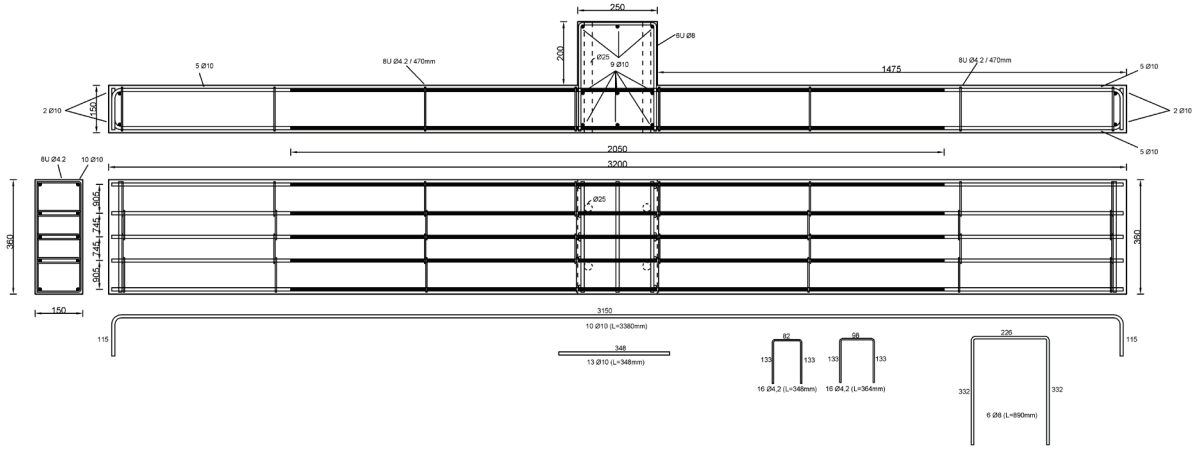

Figure 5: Unbonded reinforcement of the long span specimen.

Figure 6: Unbonded reinforcement in specimen SU-4.

The steel class used for the longitudinal reinforcement corresponds to B500A [6]. Yield strength was equal to 586 MPa, the maximum strength equal to 700 MPa, the strain at yielding point was ε_y=2.94 ‰ and the ultimate strain was equal to ε_u=3.41 %. These values were the mean values of ten specimens of steel rebar used for the longitudinal reinforcement. Similarly, the yield strength of the transverse reinforcement was calculated equal to 680 MPa.

The concrete properties were estimated by testing three cubic concrete specimens in uniaxial compression for the case of the two short beams and six cubic concrete specimens in the case of the two long beams. The strength class of concrete in the first case was estimated as C30/37 and in the second case as C25/30.

Four through holes with diameter of 25 mm were formed during casting of the specimens by using PVC pipes. The mounting of the loading device (actuator) was achieved by using threaded rods passing through the holes.

The hinge supports at the end-parts of the beams were implemented as in the case of reference [7]. After examining the hysteresis loops, a lash of 4 mm was measured in the supports of all specimens. The above mentioned information is summarized in Table 1.

	Span Length (m)	Concrete Class	Unbondment Length (cm)
S-4	1.0	C30/37	0
SU-4	1.0	C30/37	65
L-4	3.0	C25/30	0
LU-4	3.0	C25/30	205

Table 1: Specimen labeling and characteristics.

4 EXPERIMENTAL SETUP

The four beams were subjected in cyclic displacement with the use of a hydraulic piston [8]. The time-history of the imposed displacements for specimens S-4 and SU-4 is presented in Fig. 7(left) and for specimens L-4 and LU-4 is presented in Fig. 7(right). Each time-history is consisted of eighteen cycles divided into groups of three, of equal displacement. Each cycle has duration of two minutes and the total running time is 36 mins.

In Fig. 8 a sketch of the experimental setup is shown, for the case of the short beams. The cyclic displacement is imposed in the midspan of the beams, where the hydraulic actuator is attached to the rigid zone of the beams through a QHS 140x140x4 mm steel hollow beam of 460 mm length.

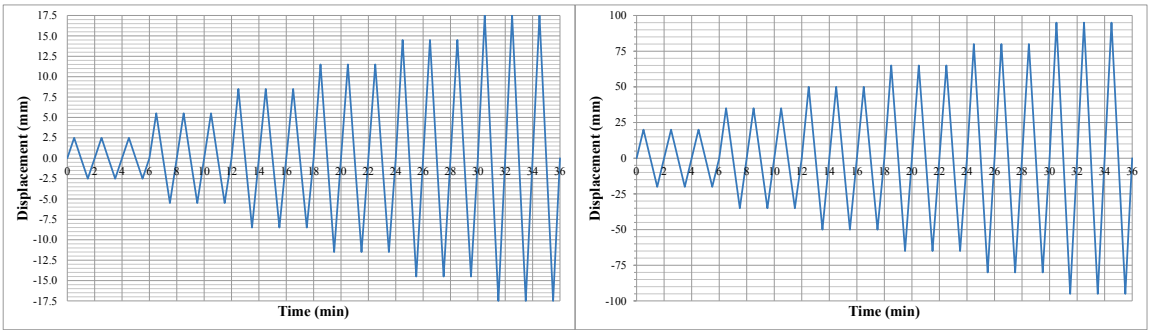

Figure 7: Imposed displacement time – histories of S-4 and SU-4 (left) and of L-4 and LU-4 (right).

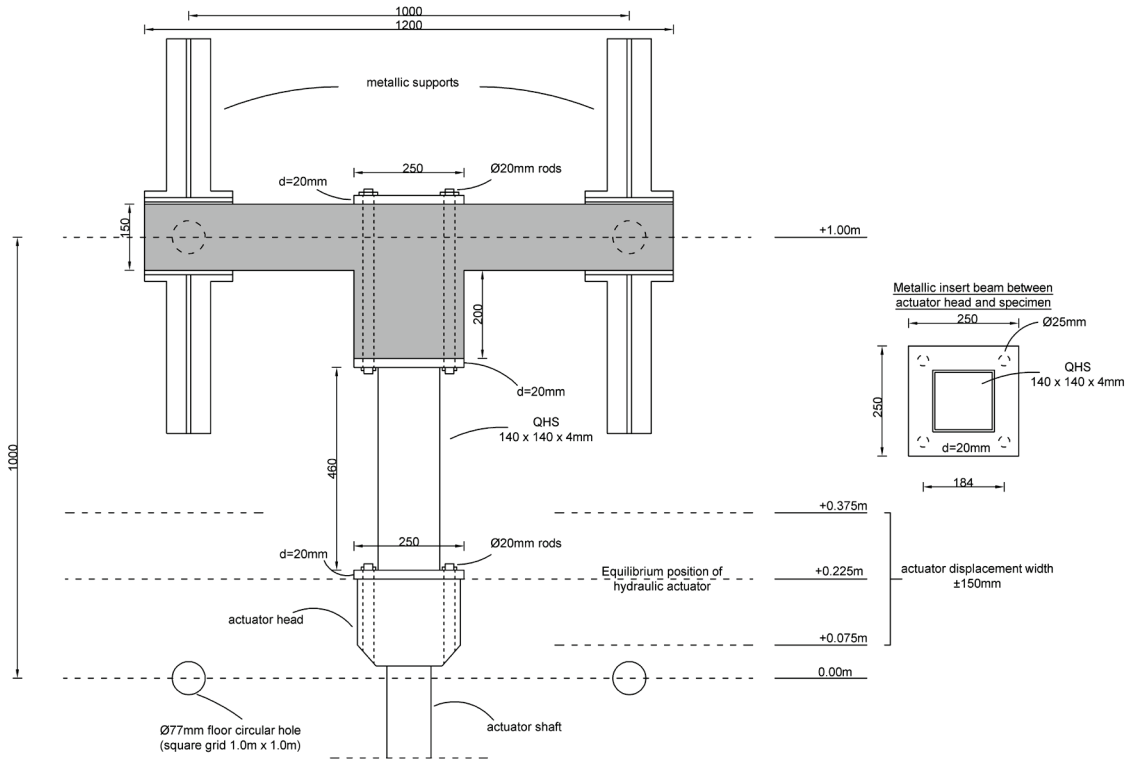

Figure 8: S-specimen position relative to the hydraulic piston.

The displacement load history was imposed by a double acting hydraulic actuator in the Laboratory of Reinforced Concrete and Masonry Structures, Department of Civil Engineering, Aristotle University of Thessaloniki. Full details of the experimental setup can be found in [7].

5 ANALYTICAL ESTIMATION OF THE SPECIMEN PROPERTIES

The analytical calculation of the specimens S-4 and L-4 properties regarding deformation and strength is presented on reference [7]. These analyses were performed using AnySection v.4.0.4 software [9]. The stress-strain law considered for the concrete behavior was the parabolic-rectangular diagram of EC2-Part 1 [6]. Regarding reinforcement steel, its stress-strain law was considered according to Park & Sampson [10]. The calculation of the effective stiffness of the specimens was based on the method described in section C.3 of EC8-Part 2 [11]. The calculation of the deformation ductility is based on the elastic-plastic behavior of a cantilever beam [7]. The results of the analytical estimation of the S-4 and L-4 specimens are presented in Table 2 and Table 3.

The yield moment of specimens SU-4 and LU-4 (and consequently their yield load and displacement) cannot be calculated in the same way due to the partial suppression of the reinforcement to concrete bond. In this case, at global (specimen) yielding, reinforcement stress remains constant in the area of the unbondment and is equal to the reinforcement yield stress. As a result, the moment in the fixed end of the cantilevers will be the yield moment. It is noted that due to reinforcement unbondment, one single crack will be formed in the point of the maximum moment, which is the fixed end of each cantilever. The width of the crack is determined by the deformation of the rebar (Fig. 9).

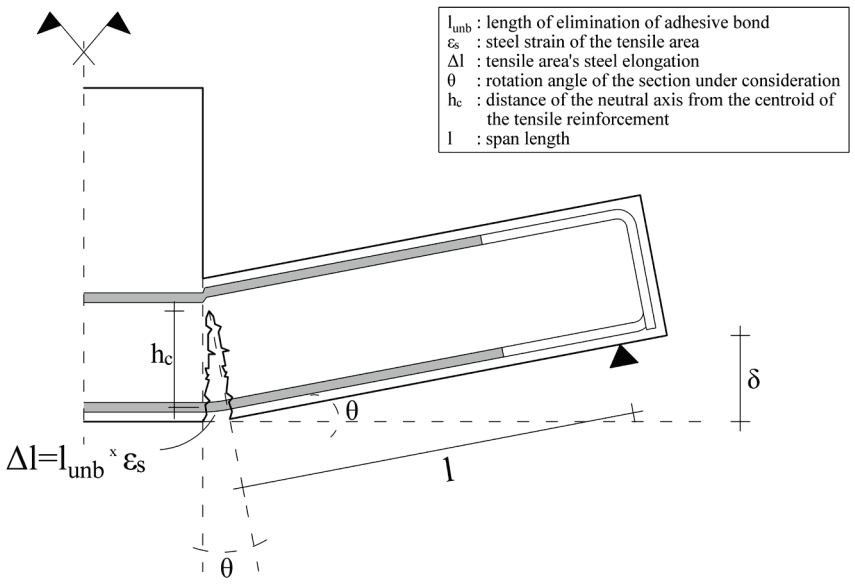

Figure 9: Schematic representation of the crack formation in the side of the rigid zone.

The crack width in each cantilever can be calculated with the following equation:

$$\Delta l = \frac{l_{unb,tot}}{2} \cdot \varepsilon_s \tag{1}$$

where $l_{unb,tot}$ is the total unbondment length. Considering that the deformation of the specimen is negligible in bonded reinforcement regions, the displacement of each specimen is calculated according to:

$$\delta = l \cdot \tan\theta \tag{2}$$

where θ is the rotation angle, equal to $\Delta l / h_c$.

The distance of the neutral axis from the centroid of the tensile reinforcement (h_c) and consequently the rotation angle (θ) were determined by modeling the section under consideration in SAP2000 [12]. More specifically, a totally rigid frame (according to the Bernoulli–Euler assumption, i.e. plane sections remain plane and perpendicular to the axis of the element) with a length of 15 cm was meshed in segments of 1 cm. In each node a non-linear spring was assigned representing the rebar or the concrete of the section (Fig. 11). The force-displacement law defined for the springs representing the concrete of the section is the parabolic-rectangular stress-deformation law of the EC2-Part 1 multiplied by the tributary area, namely 1 cm x 36 cm (Fig. 10-left). The force-displacement law defined for the springs representing the rebar of the section is the stress-deformation law according to Park & Sampson multiplied

by the area reinforcement of each spring (5Ø10), considering deformation on yielding and failure that correspond to the length of the unbonded part of reinforcement (Fig. 10-right).

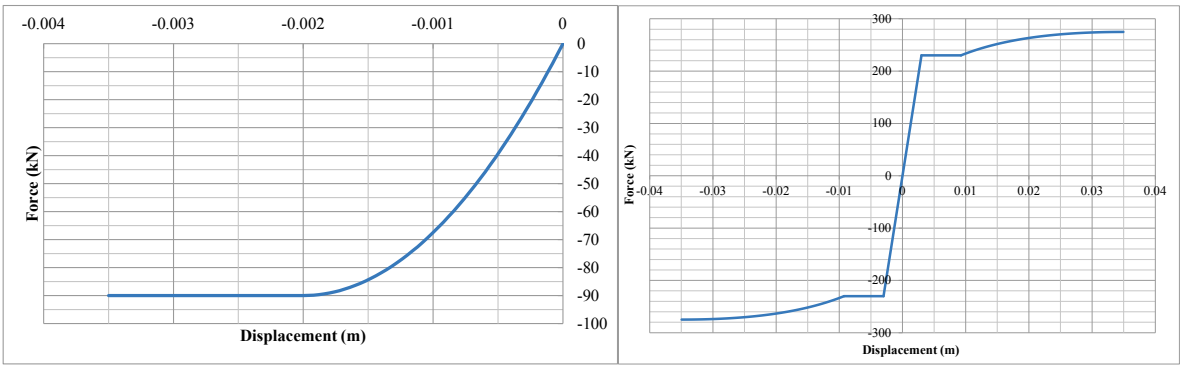

Figure 10: (Left) Sping stiffness diagram for concrete in the case of LU-4, (Right) Spring stiffness diagram for rebar in the case of LU-4

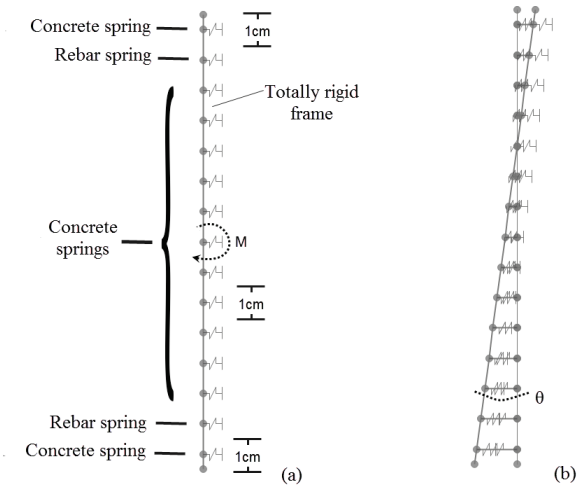

Figure 11: Finite element modelling of the section under consideration.

The type of the analysis conducted was static non-linear by gradual increase of the moment applied in the rigid frame. In both cases failure caused due to the failure of the tensile reinforcement. The moment-rotation diagrams and their bilinearization as calculated with BILIN software [13] are presented in Fig.12.

The yield load can be calculated according Fig. 12 and the yield displacement is calculated according to the equation (2). The effective stiffness can be calculated from the following equation:

$$EJ_{eff} = \frac{M_y \cdot l^2}{3\delta_y} \tag{3}$$

where l is the length of the cantilever from the side of the rigid zone to the support.

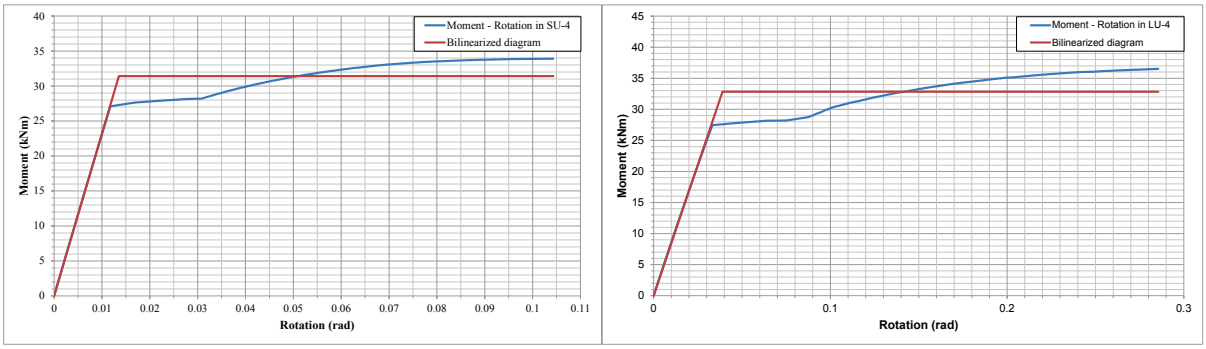

Figure 12: Moment-rotation diagrams of the critical section of SU-4 and LU-4.

The analytically calculated properties of the specimens with the unbounded parts of reinforcement are presented in Table 4 and Table 5.

M_y (kNm)	P_y (kN)	EJ_{eff}/EJ_{un} (%)	φ_y (1/m)	φ_u (1/m)	L_p (mm)	δ_y (mm)	δ_u (mm)	μ_δ
31.25	166.7	33.99	0.033	0.286	114.5	1.5	10.8	6.94

Table 2: Analytical results for the specimen S-4.

M_y (kNm)	P_y (kN)	EJ_{eff}/EJ_{un} (%)	φ_y (1/m)	φ_u (1/m)	L_p (mm)	δ_y (mm)	δ_u (mm)	μ_δ
30.85	44.9	35.03	0.034	0.288	225.4	21.2	93.6	4.41

Table 3: Analytical results for the specimen L-4.

θ_y (rad)	θ_u (rad)	M_y (kNm)	P_y (kN)	EJ_{eff}/EJ_{un} (%)	δ_y (mm)	δ_u (mm)	μ_δ
0.014	0.104	31.41	167.5	8.69	5.1	39.3	7.71

Table 4: Analytical results for the specimen SU-4.

θ_y (rad)	θ_u (rad)	M_y (kNm)	P_y (kN)	EJ_{eff}/EJ_{un} (%)	δ_y (mm)	δ_u (mm)	μ_δ
0.039	0.286	32.83	47.8	17.77	53.5	403.6	7.54

Table 5: Analytical results for the specimen LU-4.

6 EXPERIMENTAL RESULTS

Interesting results were observed during the experimental procedure regarding the three response indexes, namely, strength, stiffness and ductility. Regarding L-4, flexural cracks were observed in the area around the stiff zone of the beam, which increased along the increase of the imposed deflection and the progressive formation of plastic hinge. Crosswise cracks oc-

curred in S-4, which indicated the intense presence of shear effect (Fig. 13). However these specimens managed to deplete their flexural strength as show by the experimental results.

Regarding specimens SU-4 and LU-4 the failure mode was different from the initially supposed. In low level displacements the cracks were formed at the side of the rigid zone, like it was initially supposed (Fig. 14). Along the increase of the imposed displacements, cracks showed up in the section around the end-part of the unbonded reinforcement. This happened because stress in the unbonded part of reinforcement was of constant value. The form of the cracks in the last load cycles, during high level of imposed displacements, is presented in Fig. 15. The width of the initially supposed single crack at the side of the rigid zone was distributed into two cracks, one at the side of the rigid zone and one at the section of the end-part of the unbonded rebar. Especially, the absence of transverse reinforcement in the end-part of the unbonded rebar led to the delamination of the concrete coating and to intensive disrupt of the section concrete core (Fig. 15-right).

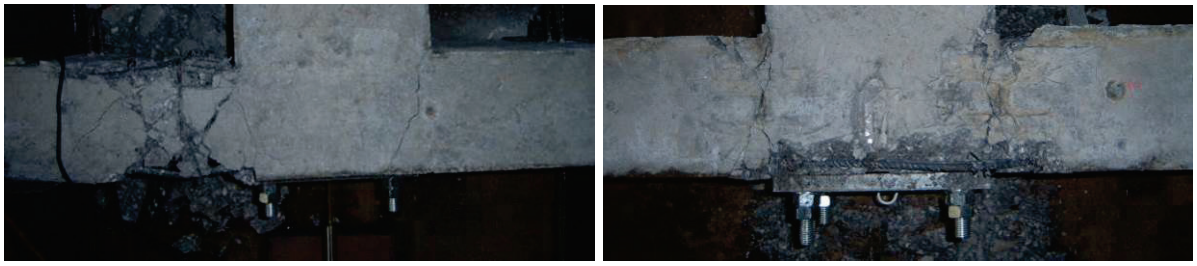

Figure 13: Crack formation in S-4 (left) and L-4 (right).

Figure 14: Crack formation at the side of the rigid zone in LU-4.

Figure 15: (Left) Crack final form in SU-4, (Right) Concrete disrupt in LU-4.

By processing the specimen hysteresis loops (Fig. 16 and Fig. 17), the results given in Table 6 were obtained. The 4 mm gap in the supports of the specimens was omitted from the

calculations and the specimens were considered as firmly mounted in the supports. It should be noted that the values of these tables are average values of both the directions of cyclic loading. Equation (4) was used for the determination of the experimental effective stiffness of the cantilevers:

$$P_y \cdot \delta_y = \int_0^L \frac{M^2_{(x)}}{EJ_{eff}} dx + \int_0^L \frac{V^2_{(x)}}{GA_s} dx \quad (4)$$

where $M_{(x)}$ and $Q_{(x)}$ are the moment and shear values of the cantilevers respectively, P_y is the half of the yield load of the beam, δ_y is the yield displacement of the beam, G is the shear modulus considering cracked concrete and A_s is the cantilevers section shear area.

	P_y (kN)	δ_y (mm)	δ_u (mm)	EJ_{eff} / EJ_{un} (%)	μ_δ
S-4	172.4	3.4	13.2	13.5	3.91
SU-4	167.8	5.7	>15.5	7.8	>2.81
L-4	44.3	19.9	>93.0	30.8	>4.67
LU-4	42.1	29.8	89.6	19.5	3.01

Table 6: Experimental results disregarding the existence of the 4 mm gap in the supports.

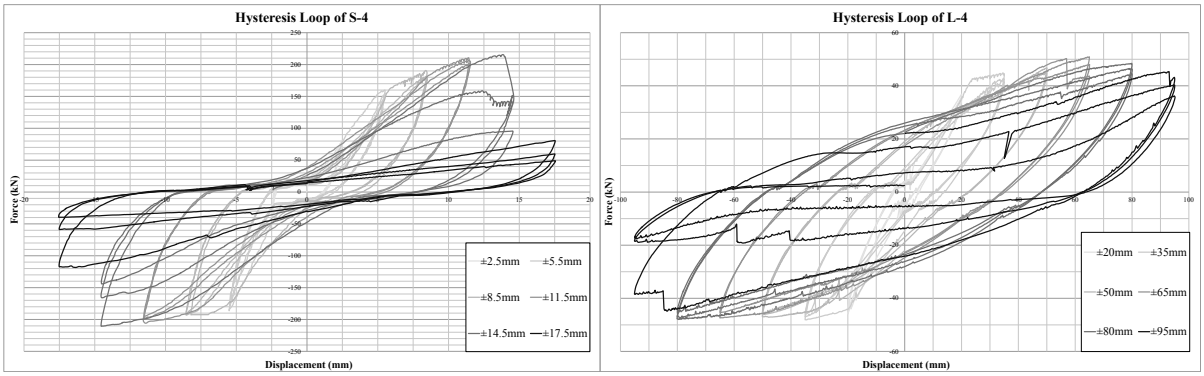

Figure 16: Hysteresis loops of the specimens S-4 and L-4.

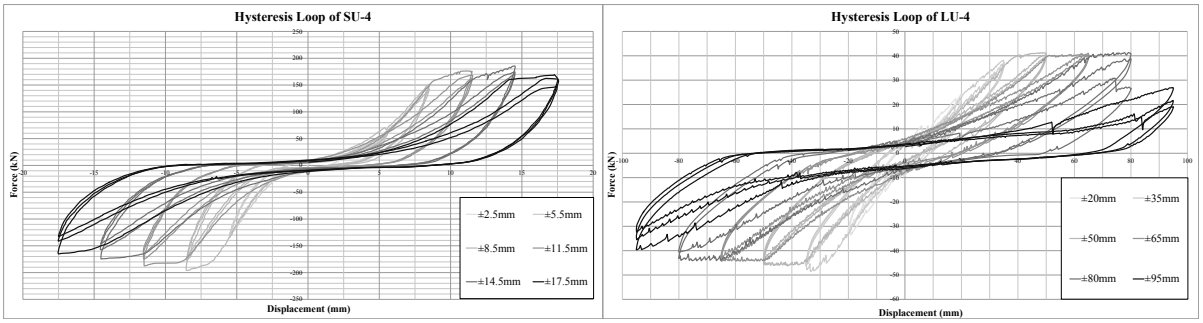

Figure 17: Hysteresis loops of the specimens SU-4 and LU-4.

By comparing the analytically calculated specimen properties with the experimental results of Table 6, regarding specimen S-4, the difference observed between the analytical and experimental results is due to the low shear span ratio of the specimen and the influence of shear stresses. Regarding L-4, the analytical results are close to the experimental. The same denotation applies for specimen SU-4. It is noted that SU-4 in contrast to LU-4 did not fail in the last

displacement level group of ±17.5 mm (by losing 20% of its strength). On the contrary, regarding specimen LU-4, the analytical results of displacements and the available displacement ductility are different from the experimentally obtained. This is due to the different mode of deformation and crack formation the specimen experienced. Initially, for the analytical calculation of its properties, the assumption of a single crack formation (at the side of the rigid zone) was made. During the experiment it was observed that a second crack formatted at the area of the end-part of the unbonded rebar. A part of the total deformation due to the rebar elongation was concentrated in that area. In addition, the absence of transverse reinforcement in that area led to the premature disrupt of the concrete. As a result of this were the lower than the expected displacements and available displacement ductility.

Comparing the results of the four specimens the following can be stated:

- The bond suppression in SU-4 and LU-4 did not seem to affect their strength, regardless of shear span ratio.
- The specimens with the unbonded reinforcement yield in larger deformations than the specimens S-4 and L-4. Therefore, their effective stiffness is significantly lower compared to the stiffness of S-4 and L-4.
- Specimen SU-4 did not reach failure. Comparing its analytically calculated available displacement ductility with the one of S-4, the first mentioned has slightly greater value. Specimen LU-4, although it was analytically expected to have almost twice the available displacement ductility of L-4, experimentally presented lower displacement ductility due to the formation of a second crack in the area of the end-part of the unbonded rebar.

The absolute values of dissipated energy and the dissipated energy per cycle (as a percentage of the dissipated energy of the first cycle of each group of the same displacement level) of specimens SU-4 and LU-4 are presented in Figures 18 and 19. The corresponding diagrams of S-4 and L-4 are presented in reference [7]. An increase of the dissipated energy is observed when imposed displacement is increasing in both cases. The percentage of the dissipated energy of the second and third cycle compared to the corresponding of the first cycle of each displacement group increases in both cases along with the increase of the imposed displacement. In the case of SU-4 this increase is not as obvious as in the case of the other specimens because this specimen was far from its failure according to Table 4 and Table 6. Specimen LU-4 corresponding dissipated energy percentage is descending in the last group of imposed displacements because of its premature failure.

Comparing the dissipated energies of SU-4 and LU-4 with the corresponding of S-4 and L-4 we observe that for the same extend of imposed displacements the second two specimens present in average 2.5 times larger amount of dissipated energy than the specimens with the unbonded reinforcement. It can be seen that specimens SU-4 and LU-4 appear to be activated in larger imposed displacements than specimens S-4 and L-4.

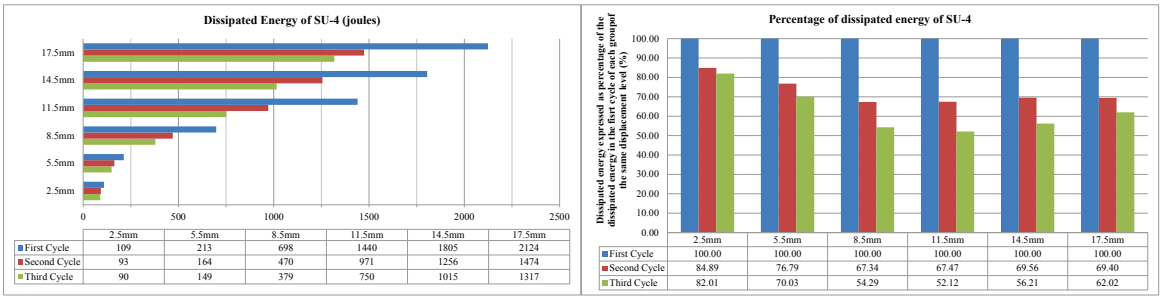

	2.5mm	5.5mm	8.5mm	11.5mm	14.5mm	17.5mm
First Cycle	109	213	698	1440	1805	2124
Second Cycle	93	164	470	971	1256	1474
Third Cycle	90	149	379	750	1015	1317

	2.5mm	5.5mm	8.5mm	11.5mm	14.5mm	17.5mm
First Cycle	100.00	100.00	100.00	100.00	100.00	100.00
Second Cycle	84.89	76.79	67.34	67.47	69.56	69.40
Third Cycle	82.01	70.03	54.29	52.12	56.21	62.02

Figure 18: Energy dissipation of specimen SU-4.

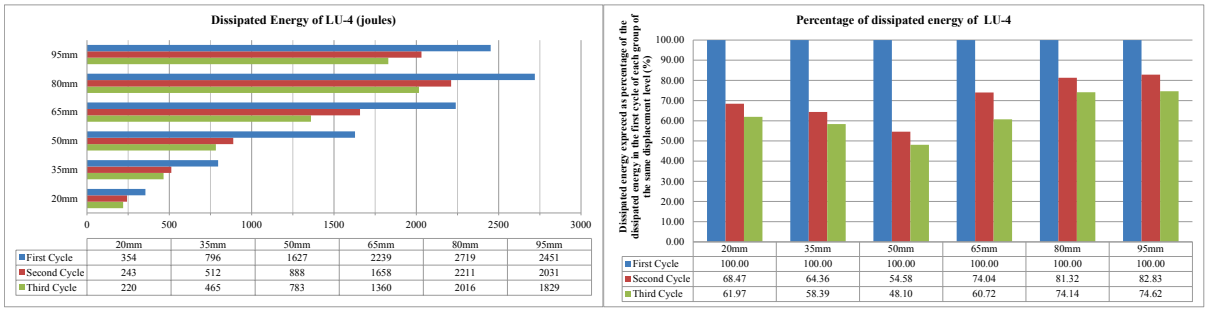

	20mm	35mm	50mm	65mm	80mm	95mm
First Cycle	354	796	1627	2239	2719	2451
Second Cycle	243	512	888	1658	2211	2031
Third Cycle	220	465	783	1360	2016	1829

	20mm	35mm	50mm	65mm	80mm	95mm
First Cycle	100.00	100.00	100.00	100.00	100.00	100.00
Second Cycle	68.47	64.36	54.58	74.04	81.32	82.83
Third Cycle	61.97	58.39	48.10	60.72	74.14	74.62

Figure 19: Energy dissipation of specimen LU-4.

The damage factor of the specimens SU-4 and LU-4 regarding the stiffness loss in each cycle [14] is given in Figure 20 and the corresponding diagrams of S-4 and L-4 are given in reference [7]. Regarding specimens S-4 and L-4, it is noted that the damage factor is constant and low, around 3 % to 5 %, except of the groups of displacement cycles that are near to the failure of the specimens. Specimen SU-4 exhibits stable performance during the consecutive cyclic imposing of displacement. On the contrary, specimen LU-4, which depletes its available displacement ductility in imposed displacement below the maximum imposed during the experiment, presents sudden loss of stiffness in the second and third cycle in displacement groups of ±14.5 mm and ±17.5 mm.

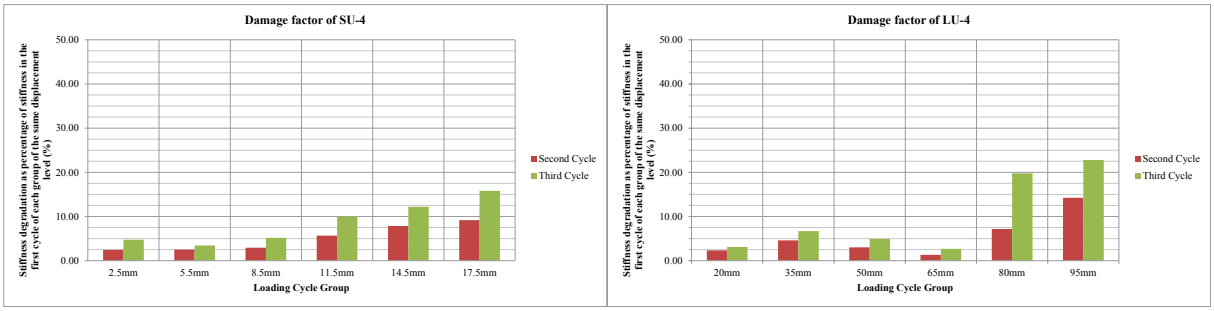

Figure 20: Damage factor (stiffness degradation) of SU-4 and LU-4.

7 CONCLUSIONS

The experimental study on the mechanical behavior of a novel type of joint connection between pier and deck or between pier and pile cap was presented in this study. In particular, three response indexes were examined namely strength, stiffness and ductility. Furthermore, the influence of longitudinal reinforcement unbonding on energy dissipation capacity and constant performance of the pier during cyclic loading was examined.

The main conclusions are as follows:

- The specimen strength, where the reinforcement to concrete bond had partially been suppressed, was slightly reduced - by 5 % - compared to the specimens without bond suppression. Therefore, it can be stated that the reinforcement partial bond suppression does not seem to significantly affect strength.
- The analytically calculated and the experimental values of the specimen effective stiffness with unbonded reinforcement were significantly degraded compared to those with regular reinforcement. In the stiff (short) and flexible (long) specimens the degradation was 42 % and 37 %, respectively. This means that reinforcement partial bond suppres-

sion renders piers more flexible and capable to withstand serviceability loads without developing major stress.

- The available displacement ductility of the short specimen (low shear span ratio) did not depleted during the maximum imposed displacement. The analytically calculated value was increased by 11 % compared to the regularly reinforced specimen. Regarding the long specimen (high shear span ratio), its available displacement ductility depleted and accrued significantly lower to the analytically calculated. A safe conclusion cannot be obtained because the failure mechanism was not the same in the two cases.
- The fact of plastic hinge formation in the area of the end-part of the unbondment leads to the conclusion that the bond suppression must not take place in the web of the piers but inside the connection joint of deck and pier or pile cap and pier.
- The amounts of dissipated energy in the case of the specimens with unbonded reinforcement are significantly lower than in the case of their ordinary counterparts, for a given size of imposed displacement. Comparing the percentage of the dissipated energy in the two cases, it is concluded that the specimens with unbonded reinforcement are activated in a higher level of imposed displacements compared to ordinary reinforcement.
- Stiffness loss in the case of specimens with unbonded reinforcement during the consecutive imposed displacement cycles is similar to the loss of specimens with ordinary reinforcement.

REFERENCES

[1] M.J.N. Priestley, F. Seible, G.M. Calvi, *Seismic Design and Retrofit of Bridges*. John Wiley & Sons Inc., 1996.

[2] M.J.N. Priestley, The PRESSS Program-Current Status and Proposed Plans for Phase III. *PCI Journal,* **41-6**, 22-40, 1996.

[3] M.J.N. Priestley, S. Sritharan, J.R. Conley, S. Pampanin, Preliminary Results and Conclusions from the PRESSS Five-story Precast Concrete Test-Building. *PCI Journal,* **44-6**, 42-67, 1999.

[4] A. Palermo, S. Pampanin, G.M. Calvi, The Use of "Controlled Rocking" in Seismic Design of Bridges. *13th World Conference on Earthquake Engineering*, Vancouver, Canada, August 1-6, 2004.

[5] I. Tegos, V. Piltisis, Th. Chrysanidis, A Proposal for the Use of a New Type of Pier Connections with Deck and Pile Cap with Financial, Functional and Seismic Advantages. *International Conference IBSBI 2014, "Innovations on Bridges and Soil-Bridge Interaction",* Athens, Greece, October 16-18, 2014.

[6] CEN [Comité Européen de Normalisation], EN 1992-1-1: Eurocode 2: Design of Concrete Structures - Part 1-1: General Rules and Rules for Buildings, 2004.

[7] V. G. Pilitsis, V.K. Papanikolaou, I.A. Tegos, K.-A. Stylianidis, A Novel Mechanism for restraining Seismic Actions in Ductile Bridges: Analytical Modeling and Experimental Verification. *5th International Conference on Computational Methods in Structural Dynamics and Earthquake Engineering,* Crete Island, Greece, May 25-27, 2015.

[8] K.-A. Stylianidis, K.V. Papanikolaou, C. Ignatakis, T. Salonikios, The Novel Cycle-Loading System of The Laboratory of Reinforced Concrete and Masonry of A.U.Th. - Potential and First Applications (Greek). *11th Greek Conference on Reinforced Concrete,* Corfu, Greece, May 18-20, 1994.

[9] V. K. Papanikolaou, *Analysis of arbitrary composite sections in biaxial bending and axial load.* Computers & Structures **98-99**, 33-54, 2012.

[10] R. Park, R.A. Sampson, *Ductility of Reinforced Concrete Column Sections in Seismic Design,* Journal of the ACI, **69-9**, 543-551, 1972.

[11] CEN [Comité Européen de Normalisation], EN 1998-2: Eurocode 8: Design of Structures for Earthquake Resistance - Part 2: Bridges, 2005.

[12] Computers and Structures Inc., *SAP2000 Nonlinear ver.11.0.3 - User's Reference Manual,* 2007.

[13] G. Panagopoulos, A.J. Kappos, Bilinear Approximations of Force - Displacement Curves. *16th Greek Conference on Reinforced Concrete,* Paphos, Cyprus, October 21-23, 2009.

[14] S.K. Kunnath, C. Jenne, Seismic Damage Assessment of Inelastic RC Structures, *5th U.S. National Conference on Earthquake Engineering*, Chicago, U.S.A., July 10-14, 1994.